Numerical analysis of Vertical Axis Wind Turbine performance at varied Angle-of-Attack

Thokozani Justin Kunene
Mechanical & Industrial Engineering Technology Department
University of Johannesburg, Doornfontein Campus
Johannesburg, South Africa
tkunene@uj.ac.za

Mossa Maculove
Mechanical & Industrial Engineering Technology Department
University of Johannesburg, Doornfontein Campus
Johannesburg, South Africa
217012818@student.uj.ac.za

Lagouge Kwanda Tartibu
Mechanical & Industrial Engineering Technology Department
University of Johannesburg, Doornfontein Campus
Johannesburg, South Africa
ltartibu@uj.ac.za

Abstract

A vertical axis wind turbine (VAWT) is the type of turbine that uses aerodynamic drag to rotate vertically and generate electrical energy. Wind energy is considered an important renewable energy source and the development of VAWTs is ever increasing. A household application of VAWT as a complementary energy source is considered. The study focused on the analysis of the performance of VAWTs at varied blade Angle-of-Attack (AoA). Two NACA Selig/Giguere series aerofoils were modelled for varied thicknesses and chord lengths to analyze the power of the turbine at different AoA using Computational Fluid Dynamics (CFD). A Dynamic mesh technique in the ANSYS Fluent 2019 R1 commercial software was used to model a three-H-shape VAWT that simulated a varied AoA as cam would on pivoting blades was effected through a User-Defined-Function. The varying AoA produce a higher momentum deficit in the wake, but also a faster wake recovery. The AoA reaches both the minima and maxima of the power it can produce before stalling wind over the aerofoil and forming large vortex shedding and wakes behind each blade that should have been less from a low-speed VAWT. Consequently increasing noise levels which is undesirable for urban applications. The varied AoA show a bimodal distribution of vortex shedding retracting from the blades.

Keywords

Angle-of-Attack, Computational Fluid Dynamics, Dynamic mesh, Renewable energy, Power coefficient

1. Introduction

Wind energy is progressively becoming popular and competitive in the arena of renewable energies. It holds much of its technology and potency from the aerodynamic principles which makes it much attractive for aeronautical and mechanical engineers to contribute towards the generation of electricity. The continuous development of wind energy is ever becoming important to meet the EU's 2050 low carbon economy objectives (Nguyen, et al., 2020). Now, wind energy is best captured, utilised and harnessed through the means of a wind turbine. Wind turbines are catalogued primarily to how the rotational axis is orientated. Their classification can be classified as horizontal axis wind turbines (HAWTs) and vertical axis wind turbines (VAWTs) (Peng, et al., 2020). It has been determined and the

development of Savonius and Darrieus rotors, that they are best suited for VAWTs (Jha, 2011). The three-bladed H-type of VAWTs hold some few disadvantages like they do not self-start compared to Savonius-type and generally produce less electricity the horizontal turbine (Marinic-Kragic, et al., 2019).

Now, up to 5 kW small-scale installation, VAWTs can be suitably used in a household as a complementary energy source (Fadil, et al., 2017). It means that a 12 V operation can be possible from a VAWT servicing a house requiring energy consumption from 2 kWh per day to 120 V for 20 kWh per day (Jha, 2011). An off-grid solution is, therefore, possible as there is an opportunity to have a hybrid (solar & wind), cost-effective solution running from one inverter unit for both solar and wind power modules. VAWT essentially generate low noise levels because they have slower rotations. They reduce the risk of blades from being ejected which conceals the safety and health aspects that cannot be ignored in a densely populated area (Hansen, 2008). The VAWTs reduce shadow casting and bird-killing of birds as would be required for household communities (Abraham, et al., 2012). However, no two or conservative VAWTs can be mounted even for the household application (Shaheen & Abdallah, 2016).

The main reason that power would be lost on the second or the next VAWT because produces high dynamic stalls behind it which makes wake flows. It makes the immediate VAWT to be influenced by this wake flow as it would be experiencing high turbulent intensity (Zuo, et al., 2016). It is noticeable, therefore, to reduce the wake effect space or distance the wind turbines would need to be large enough which would defeat the purpose of VAWT being useful for households. It almost seems less practical to install VAWT, even at small scale, for a household because rotors of wind turbines are normally placed on towers or raised high enough where stronger winds are available. Yet, there is a great opportunity to further improve the designs of the VAWT such that they would remain fully operational and optimal for all known wind conditions.

The topic is certainly not new or ground-breaking. It was visited extensively Elkhoury *et al* where the performed experiments using a wind tunnel and a superior numerical method of the large eddy simulation (LES) with dynamic smagorinsky subgrid-scale (SGS) modelling (Elkhoury, et al., 2015). We present a system that, by a simple bearing configuration on the blade in a form of yaw system, effect the rotor speed to suit changing wind directions. It addresses pitch control, where the pitch of the blades are varied to ensure maximum power is reached and the passive stall is minimised. We will use a blade pitch adjustment that maximises the power out over the same sweep area. We set numerical simulations of the varying AOA over two different NACA Selig/Giguere series aerofoils on a three-bladed H-type VAWT using the much popular and preferred one-equation turbulence model in aerodynamics; the Spalart-Allmaras model. We will track a power coefficient, for a rated wind energy case only. This approach applied to all the derivatives as mentioned in this introduction for low normalised wind speed usually found within resident communities.

2. Computational methodology

2.1. Geometry and topology of VAWT

Figure 1 shows the main components of VAWTs which are fixed and varied blades. In this paper, we present a system that, by a simple bearing configuration on the blade in a form of yaw system, effect the rotor speed to suit changing wind directions in to capture is energy and maximise a lift force with each revolution. Figure 1b depicts a pitch control system enabled by a cam system that is located at the centre of the blade. Now the modelling a sinusoidal profiled that both limits the blade's angle to a good degree where static stall of the wind energy can be avoided. Yet, enough not to cause drag when the blade, against the incoming wind, would be like a semi-circle object bluffing the incoming stream and increasing pressure drag on the body. In this case, this is undesirable and we attempt to minimise it to increase the velocity of the fluid.

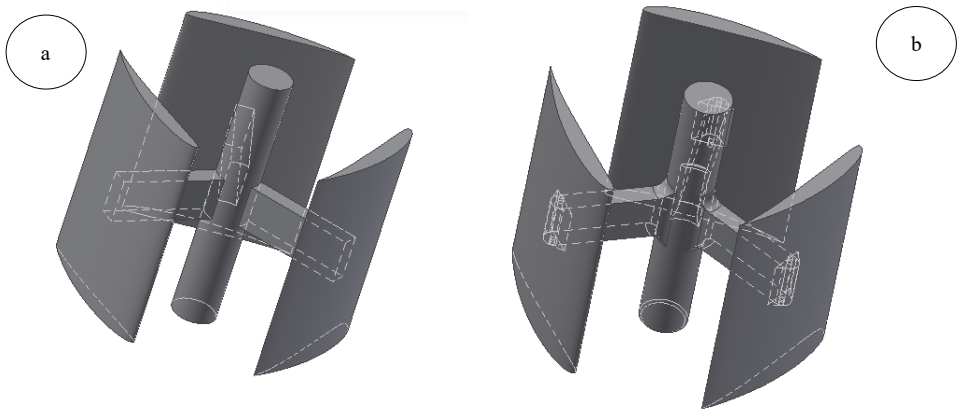

Figure 1 Three-blade H-type VAWT, rigid (fixed AOA) and swivel (varied AoA, sinusoidal profiled)

In Figure 2b the shows the NACA SG6042 and NACA SG6043 with a chord length of 0.5 m and 0.35 m respectively. The choice of the Selig / Giguere series wind turbine aerofoil is motived by its low speed. The thickness and camber are two parameters that have a great impact on the aerodynamics performance. They limit the dynamic stall of blade Reynolds number, Re_b = 771 707 at an azimuth angle, $\theta = 1.5^0$ of the blades (or rotating core in this case) when the rotation reaches 1 second. This blade Reynolds number is found on a fixed tip speed ratio, $\lambda = 0.56$. It places the blades out of the static stall (Rezaeiha, et al., 2017). The modelled blades have a maximum a 0.962^0. Rezaeiha *et al* (Rezaeiha, et al., 2017) provide the equations, i.e., eq. 1, 2 and 3, to compute stall angle and the maximum angle-of-attack.

$$W_{geo} = U_\infty \sqrt{\lambda^2 + 2\lambda\, cos\theta + 1} \quad (1)$$

$$Re_{geo} = W_{geo} c / V_\infty \quad (2)$$

$$\beta_{geo} = tan^{-1}\left[\frac{sin\,\theta}{\cos\theta + \lambda}\right] \quad (3)$$

$$\lambda = R\omega / U_\infty \quad (4)$$

Where W_{geo} is the velocity over the blade, Re_{geo} is the blades' Reynolds number. The TSR (λ) is low-speed tip ratio which has been maintained be the same for all the NACA Selig/Giguere series that were being investigated. R the rotor radius (R = 0.6 m). The upstream wind speed, U_∞ are 15 m/s and the angular speed, ω is 14 rad/s.

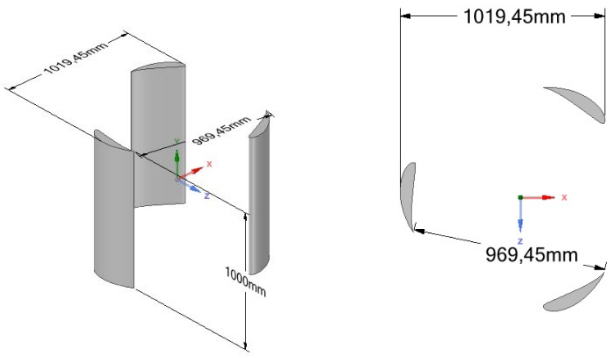

(a)

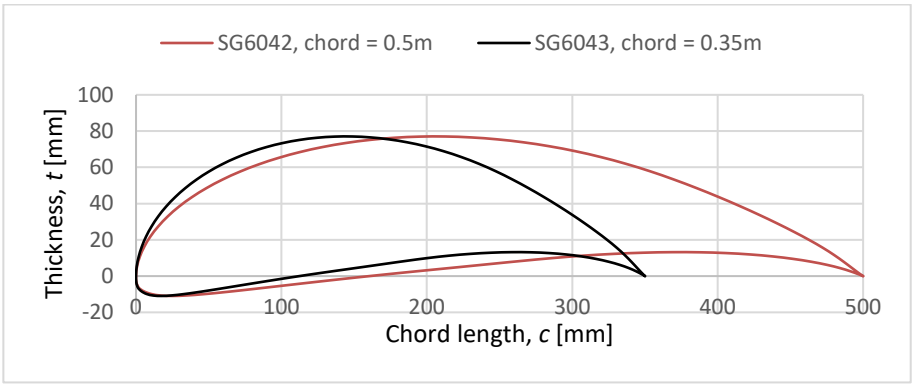

(b)

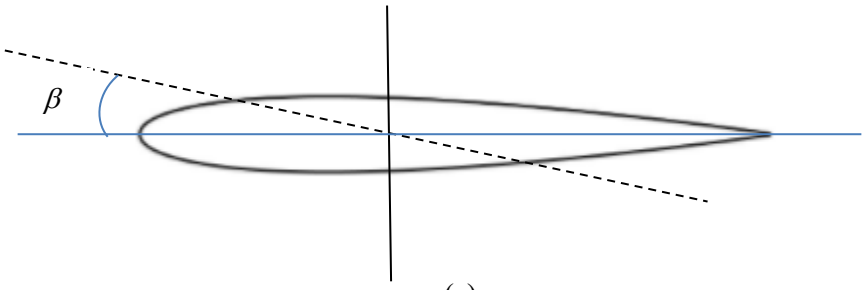

(c)

Figure 2. Detailed three-blade H-type VAWT with removed rotational arms a fixed sweep area, Selig / Giguere series low-speed wind turbine aerofoil and schematic presentation of azimuthal pitch angle

2.2. Computational domain and boundary conditions

The computational domain shown in Figure 3 consists of a rotating core is located 5D downstream the inlet. It revolves the blades from a fixed domain neighbouring the core that has a coupled interface that slides in between the fixed domain. The far-field is 30D downstream the rotating core. The far-field boundary conditions of this study were that the inflow condition a velocity inlet of 15 m/s as would be a wind speed on around residential (Jha, 2011) (Al-Shemmeri, 2010). The rotating core rotates the blades at an angular speed of, Ω = 14 rad/sec. The downwind of the computational fluid domain was specified as an outflow, i.e. zero pressure (P = 0). A turbulence intensity of 10% was maintained throughout all the scenarios to make the flow field irregular from the beginning of the simulations.

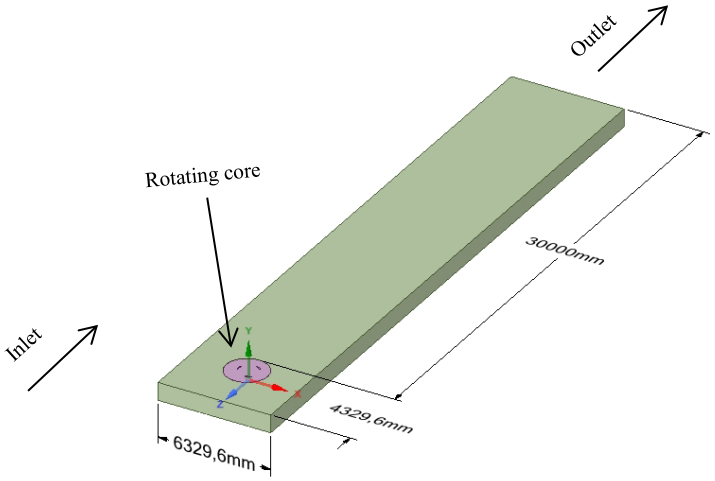

Figure 3. Far-field computational domain

The torque at this point is expected to be to decrease compared to what would have been if the incoming flow was laminar (Siddiqui, et al., 2015). The rotor dynamic zone has blades only. The struts, hub and cams were not modelled.

2.3. Mesh and grid sensitivity

Figure 4 shows the mesh generated using the body-influence which is a means to refine local bodies like the rotating core where the blades are located. Then the stationary body around is coarsened with each refinement of the rotating core. Included is the interface between the rotating core and the stationary body.

Table 1. Computation grid of the VAWT

Grid	Tetrahedral cells	Blades, y+
Course	921,765	70
Medium	1,031,431	25
Fine	2,321,748	5

Table 1 lists the mesh cells as they are being refined progressively with smaller grid sizes. The mesh density in the boundary layers had a non-dimensional wall distance to the thickness of the first layer of $1x10^{-5}$ m from 12 prismatic layers leading up to the wall plus value of, $y^+ = 5$.

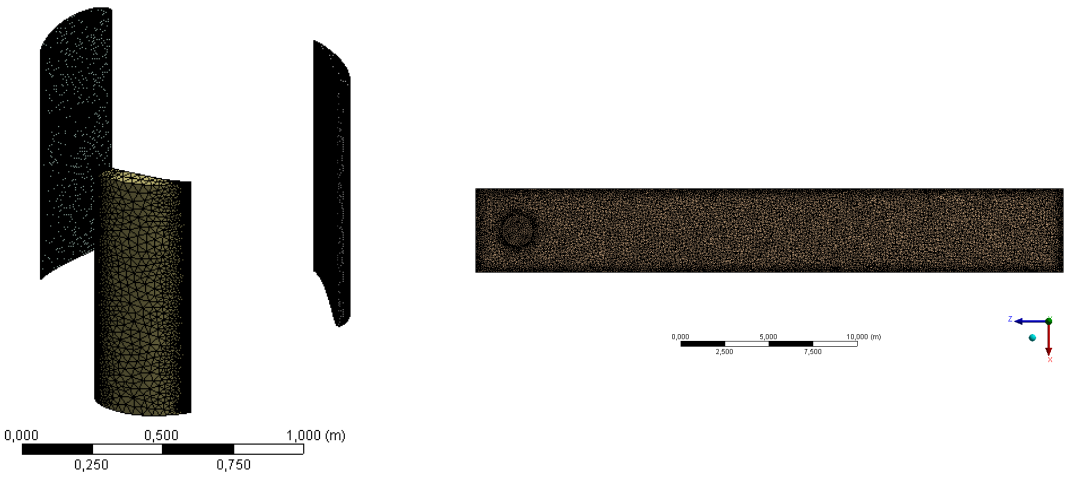

Figure 4. Mesh density of the model, tetrahedral elements

2.4. Solver and turbulence model

The incompressible unsteady Reynolds-averaged Navier-Stokes (URANS) simulations were solved using the commercial CFD code ANSYS Fluent 2019 R1. A SIMPLE scheme is used for pressure-velocity coupling. A Second-order accurate Finite Volume Method (FVM) spatial discretization was used (Rezaeiha, et al., 2017). A transient solution was adopted to capture sources that are time-dependent turbulent quantities like the vortex stretching behind the aerofoils. The convergence criterion was specified on all residuals to decrease to $1x10^{-9}$ for all the governing equations. The temporal discretisation for this unsteady flow problem required a solution that a dynamic condition will rotate blades and extract energy from the incoming stream (Satio, et al., 2018). For that actuation, a Dynamic Mesh and adapted mesh to 2 cells around each blade were used. It was considered that some mesh cells would experience negative meshing. It was important to properly match all the parameters. The affected parameters included a time step (Δt) that was set to the time required to complete an azimuthal increment ($d\theta = 1\ x10^{-5}$) degrees, blade rotation, $\Delta t = 1x10^{-5}$ s with $1x10^{+5}$ number of iterations (Rezaeiha, et al., 2018).

Two distinct User-Defined-Functions (UDF), see Appendices A and B, were used for interpreted 6-degree freedom function of all three blades rotating and a compiled UDF (centre of gravity, C_G Motion for rotation) of sinusoidal pitching of the blades (ANSYS Release 14, 2011). This UDF assimilates the changing pitch angles (β, Angles-of-Attack) of the blades which be a bearing between the rotor arm and the blade, see Figure 5b. Figure 5a also shows the motion of the blades beginning with the negative z-axis part rotation and continued positive rotation to a period of 1 second and reaching a maximum degree of rotation of 1.5^0. Further explanation of this motion will be available in the results and discussion section of this paper.

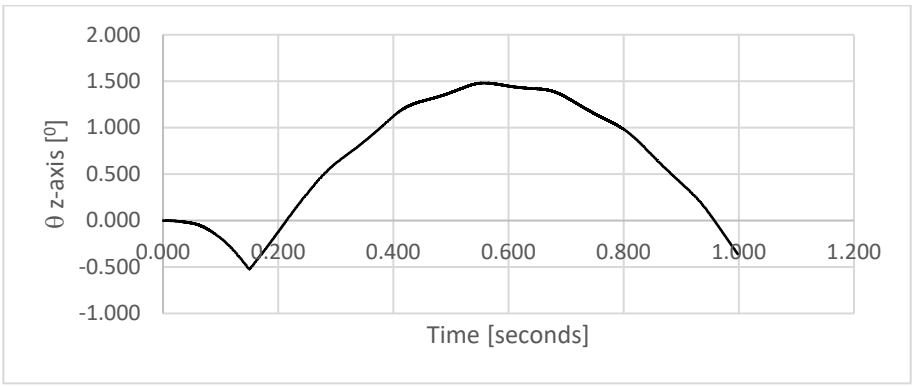

(a)

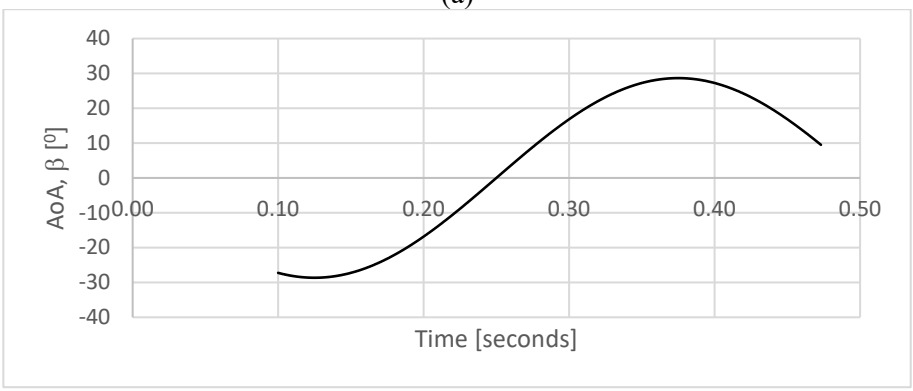

(b)

Figure 5. (a)Azimuth angle (six-degree-freedom) rotation of the blades over time-lapsed, (b) Pitch angle of the blades, β per time

2.5. Model validation

There are still few 3D simulations for all the available and possible investigations surrounding VAWT and to aerofoils, in general, The 3D simulations provides a degree of freedom that exists in reality;

account for the flow passing in an axial vertical direction even when we have omitted the rotor arms. This approach reduces the artificial blockage observed in the 2D simulations (Franchina, et al., 2019). The choice of a turbulence model this study selected was the Spalart-Allmaras (S-A model). The SA one-dimensional equations are well articulated by Kostic (Kostic, 2015) and not necessary rewritten in this paper. The incompressible RANS-SA equations as adopted in this paper referred to D'Alessandro *et al* on their numerical modelling of wind over the aerofoils (D'Alessandro, et al., 2017). Overall, the S-A model maintains good stability and rapid convergence for the pressure-gradient- driven boundary layer flows (Zhou, et al., 2017).

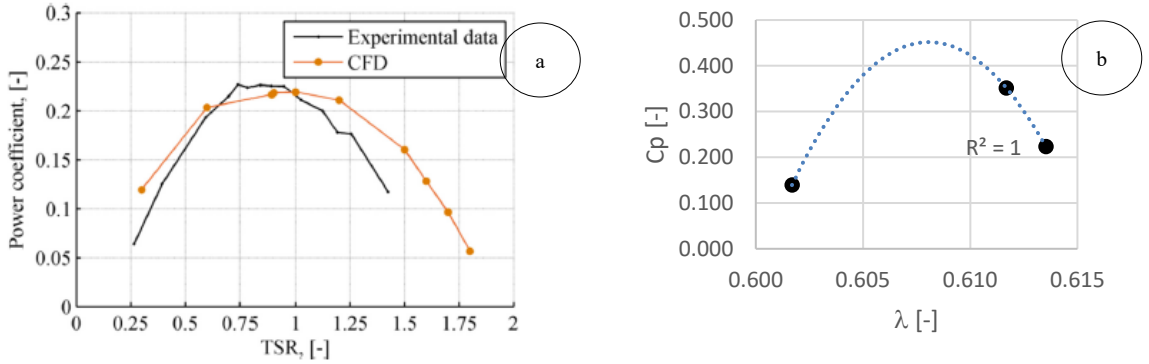

Figure 6. Comparison literature, (a) *(Marinic-Kragic, et al., 2019)* **(b) current CFD study**

The S-A model employees a one equation model that is specially designed for aerospace applications. It easily solves a modelled transport equation for kinematic eddy viscosity. It accomplished this modelling without the need to calculate the length scale that relates to the shear layer thickness. Shukla and Kavit presented the S-A model the equations as they evaluated profile modifications of straight blade VAWT (Shukla & Kaviti, 2017). The simulations were carried out in the computer cluster at the Centre for High Performance Computing (CHPC).

3. Results and discussion

The majority of the analysis of these results is based on the wind speed U_∞ is constant in time, $t = 1$ sec where the rotation has a 1.5^0 azimuth angle (unless stated). It becomes obvious that the proposed optimization of the modelled VAWT at this wind speed can be further analysed when the transient time increased. Since in practice wind speed is not constant, however, an optimum design is seen very much probable for an improved energy production.

3.1. Power performance and rated tip speed ratio

The power coefficient (C_p) is defined as (Marinic-Kragic, et al., 2019) for VAWT's is a strong indicator of performance of the turbine. Figure 6b is the power coefficient of 0.35 for a fixed angle-of-attack model has its maximum power output at a TSR of 0.613. Therefore, suggesting that is the wind speed was constant instead of fluctuating. The aerodynamic power can be increased by increasing the TSR. The VAWT to operate at its optimum point. It must be designed on the maximum point or conditions of Cp.

$$C_p = P/(\rho v^3\, A/2) \quad (4)$$

Where P is the power generated by the VAWT at an air density of $\rho = 1.22$ kg/m^3. A is the rotor swept area, $A = 2RH$. H ($H = 1$ m) is the rotor height. Figure 7 is the combination of plots showing the streamlines where are parallel being streamwise with blade 3. It shows the areas between the blades where swirls exist and low velocity-high pressure regions and the blades rotate.

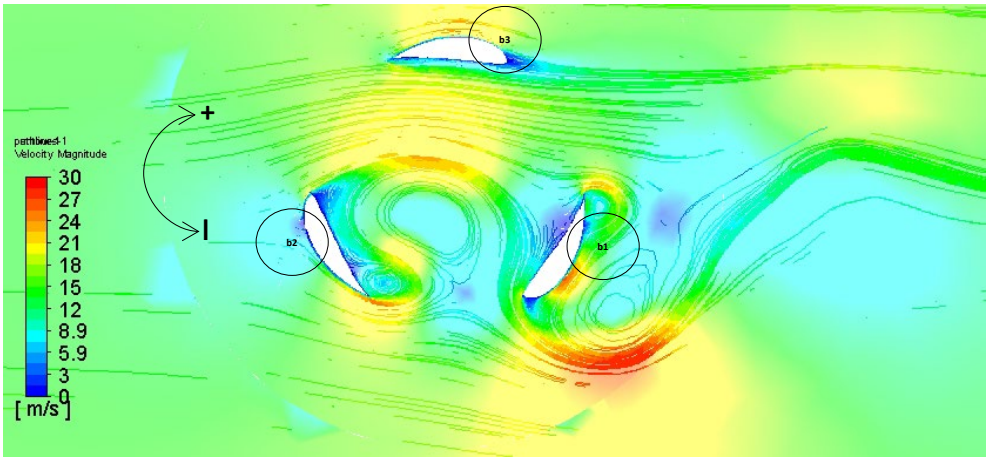

Figure 7. Velocity distribution on the symmetry plane, varied AoA, t = 1 sec

3.2. Impact of varied aerofoils on aerodynamics

The aerodynamic performance of the Selig/Gigures aerofoils is represented in Figure 8. The velocity plots are on the low pressure side of the aerofoil, chord-wise speed. The difference between the aerofoils is that SG6043 has a longer cord length than SG6043. Where all together, it can be deduced their thickness is almost the same. SG6043 transfers more energy between the blades and the fluids on all blades. The extra chord length turns to make the aerofoil slender making it to minimise the losses because of the curvature of camber line and the asymmetric distribution of its thin and cascading thickness and provides more lift force. When tracking the blade-three (b3), since VAWT are designed to operate at one point only (Hansen, 2008). It this range of time before the expected 1.5^0 turn at 1 second. The AoA appears to be optimum along the entire span of both types of aerofoils. Therefore, on the 1.5^0 azimuth angle b3 is the blade that produces a power turn.

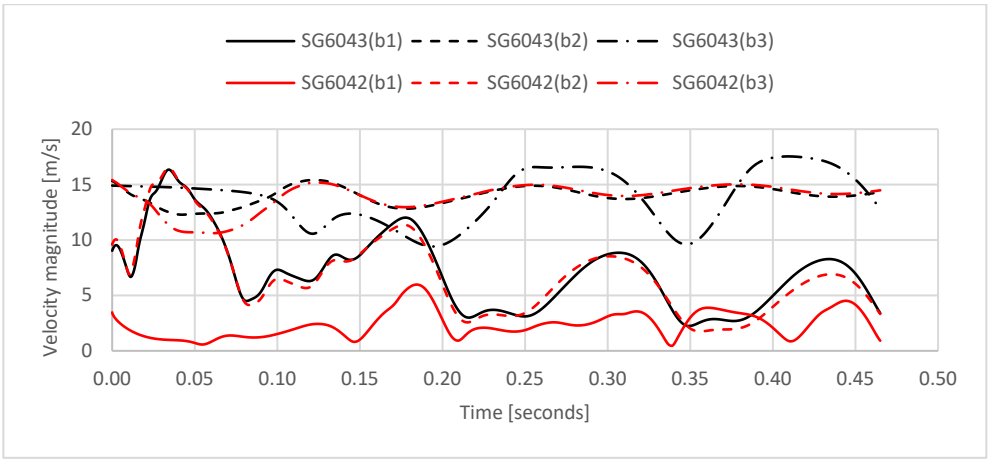

Figure 8. Wind energy capture of Selig/Giguere series aerofoils on the three blades

In Figure 9, the SG6042 aerofoil almost maintains the upstream wind speed over time. The SG6043 after some 0.25 sec losses energy then recovers it. Then periodically repeats the same pattern within a revolution. Since the measurement is along with the chord-wise speed. The rotational effects of centrifugal and Coriolis forces are influence rotating blades (Corten, 2001).

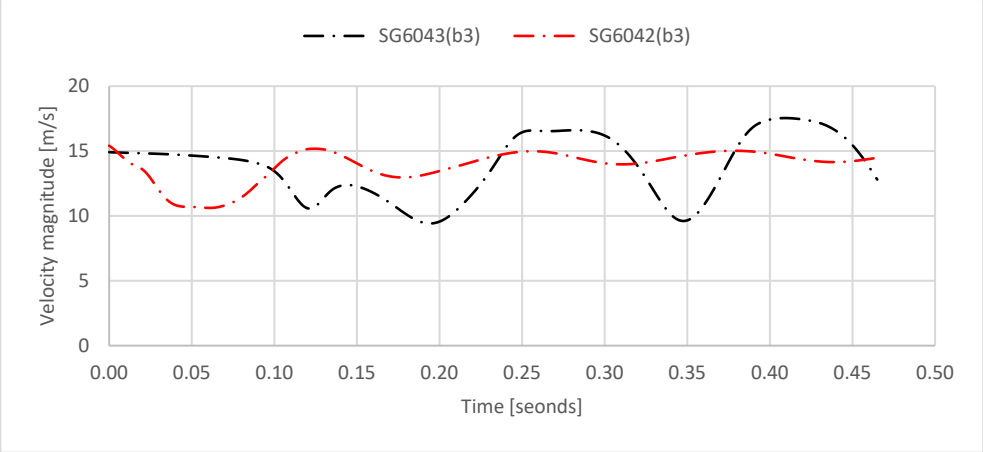

Figure 9. Blade 3 of the SG6042, c = 0.35 m and SG6043, c = 0.5 m

3.3. Impact of varied AoA

The impact of varied AoA is presented in Figure 10. Blades, b1 and b2, have shown many improvements compared to each period in Figure in enhancing streamwise wind. The blades varied AoA improves the stall behaviour within the range of low tip-speed ratios (Chen, et al., 2018).

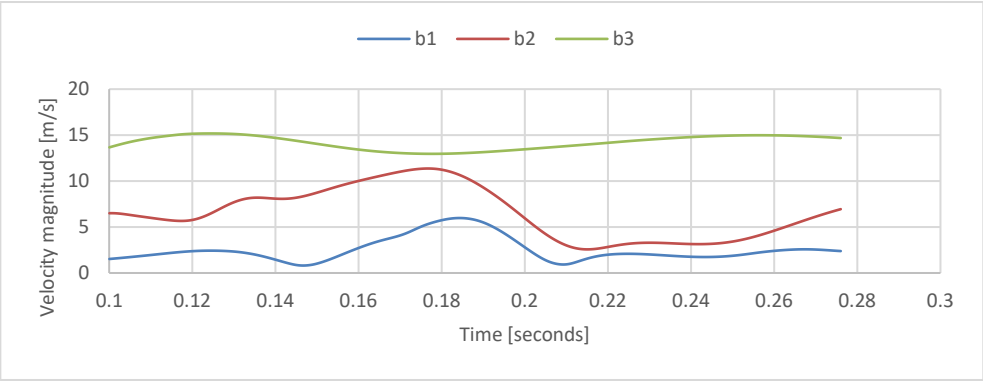

(a)

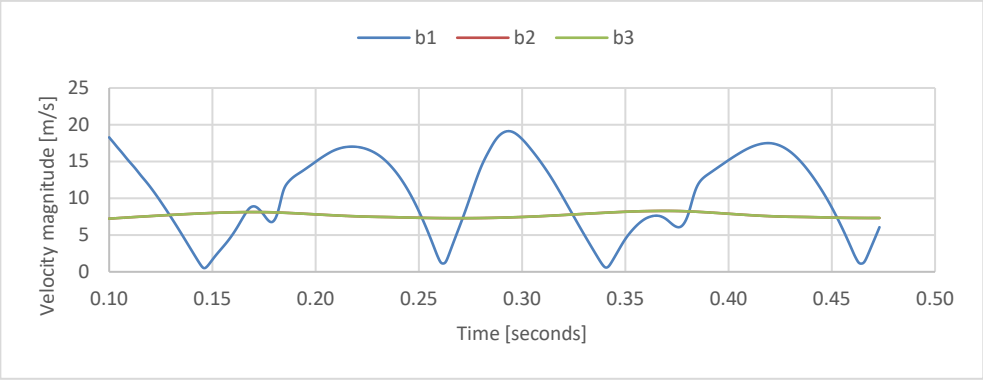

(b)

Figure 10. SG6043, (a) fixed AoA, β = 0 and (b) varied AoA, $-30^0 < \beta < -30^0$

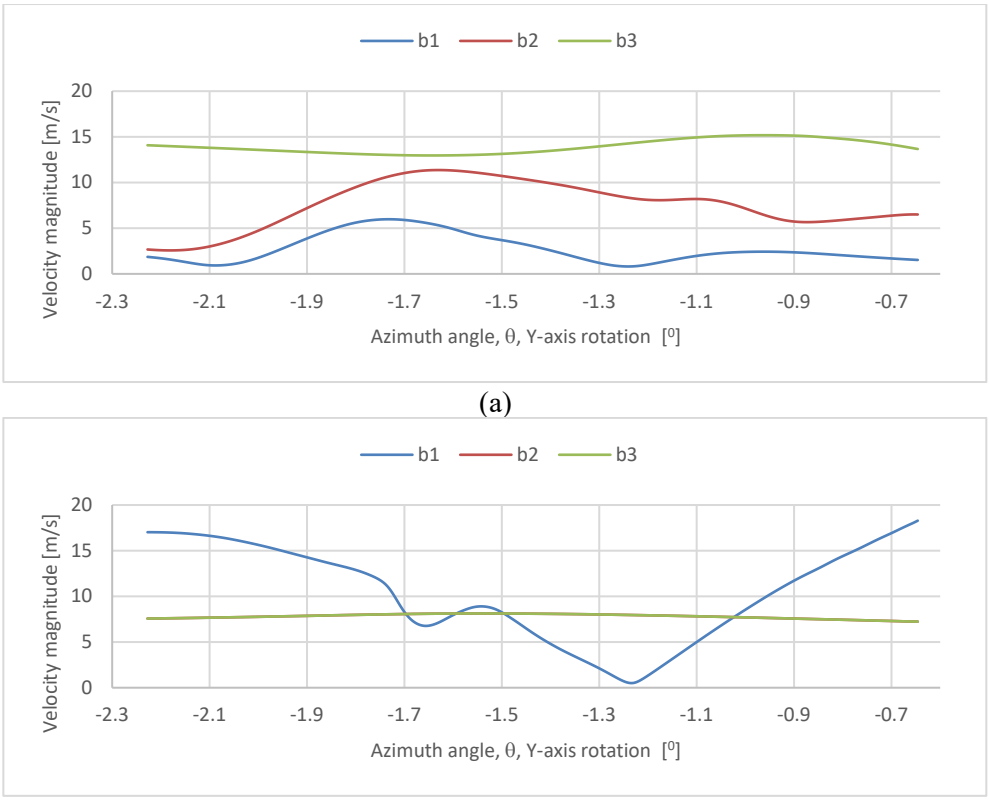

(a)

Figure 11. The azimuth angle of the rotating blades

VAWT blades experience different angles relative to their wind direction during the rotation. Figure 11a shows that the velocity generated by each blade is a function of the azimuthal position is mostly constant on fixed AoA. The varied AoA and its azimuthal position are shown in Figure 13b where velocity is stalled at about 1.25^0 (anticlockwise) which is closer to the single turn of the blades. It demonstrates how it overcame the static stall when other blades, b2 and b3, maintained a constant velocity.

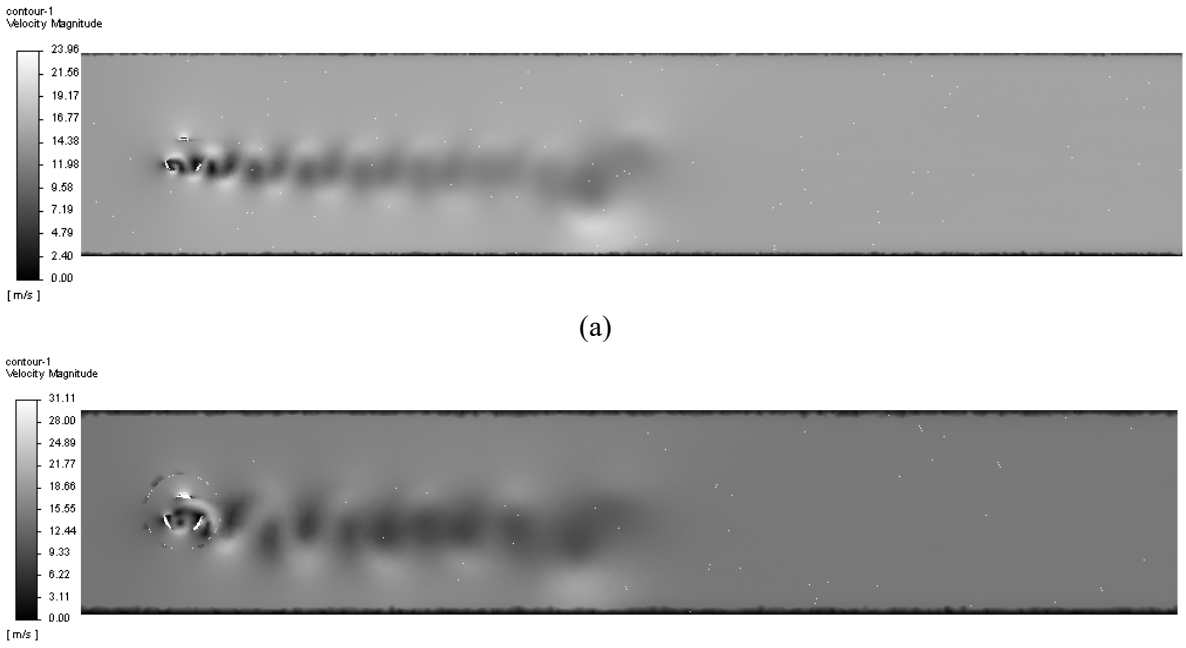

(b)

Figure 12 Von Karman velocity sheet (a) β = 0; (b) $-30^0 < \beta < -30^0$

Figure 12b, the vortex at the trailing edge separation from the leading edge is less on the varied AoA. Figure 13a shows that vortex sheets downstream the blades to be stronger and travelling further when on fixed AoA. This is another indication of the varied AoA to lower the stall separation. Therefore, the vortex sheet from varied AoA are quieter

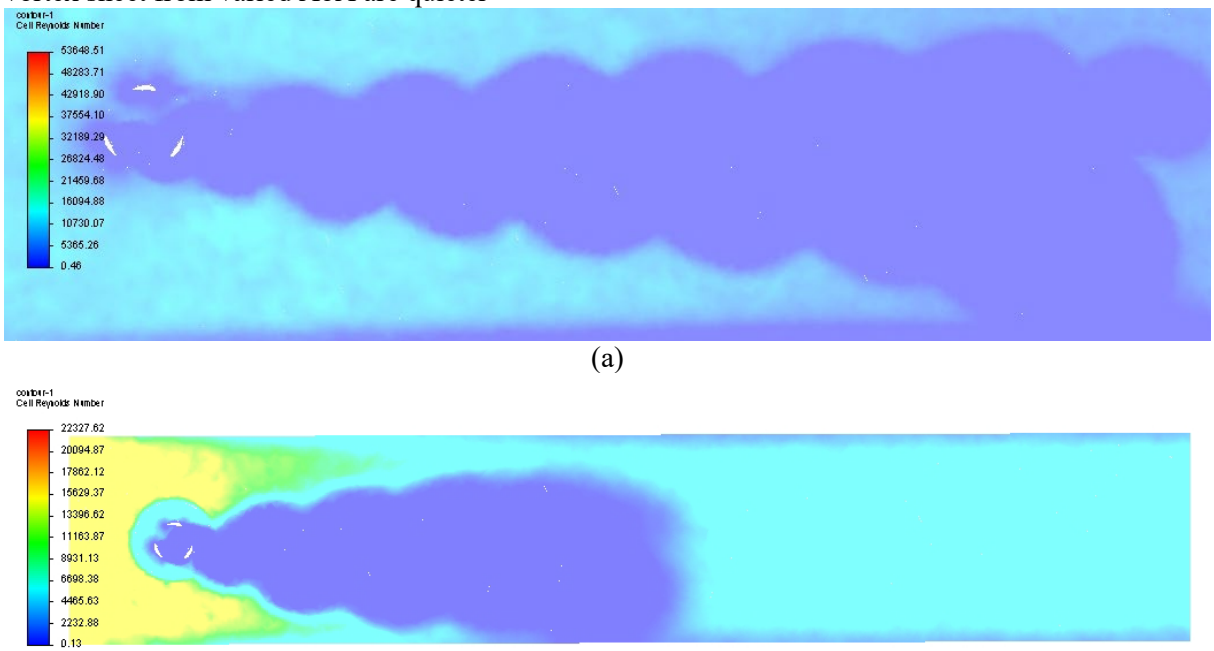

Figure 13. Reynolds number at t = 0.975 sec, (a) β = 0; (b) $-30^0 < \beta < -30^0$

In Figure 13b, the vortex at the trailing edge separation from the leading edge is less on the varied AoA. Figure 13a shows that vortex sheets downstream the blades to be stronger and travelling further when on fixed AoA. This is another indication of the varied AoA to lower the stall separation. Therefore, the vortex sheet from varied AoA is quieter too. The varied AoA reduces flow separation and weakening the instability that periodically generates separation vortices, which leads to the vibration of rotating machinery and noise generation (Liu, et al., 2019).

4. Conclusion

The potential use of varied angle-of-attack in VAWT and has been numerically investigated. The power coefficient C_p in VAWT is maximum at very low values of TSR ($\lambda = 0.6$). The results show that blade of SG6043 aerofoil with a chord length of, $c = 0.5$m yields the best energy capture in presence of varied or fixed angle-of-attack. The noise caused as demonstrated by the vortex sheet is noted but not fully modelled and analysed in this study. The observation is that the noise level and distribution is reduced on varied AoA of the blades. However, future work is needed to address the limitations of the current the study that includes range to revolutions of the turbine and for the azimuthal increment over 360^0 revolutions.

5. References

Abraham, J. P. et al., 2012. Summary of Savonius wind turbine development and future applications for small-scale power generation. Journal of Renewable and Sustainable Energy, IV(4), pp. 3-5.

Al-Shemmeri, T., 2010. Wind turbines. ISBN 978-87-7681-692-6: T. Al-Shemmeri & Ventus.

ANSYS Release 14, 2011. ANSYS FLUENT UDF Manual, s.l.: ANSYS.

Chen, B., Su, S., Viola, i. M. & Greated, C. A., 2018. Numerical investigation of vertical-axis tidal turbines with sinusoidal pitching blades. Ocean Engineering, Volume 155, pp. 75-87.

Corten, G. P., 2001. Flow separation on wind turbine blades. The Netherlands: PhD thesis, Utrecht University.

D'Alessandro, V., Montelpare, S., Ricci, R. & Zoppi, A., 2017. Numerical modeling of the flow over wind turbine airfoils by means of Spalart–Allmaras local correlation based transition model. Energy, Volume 130, pp. 402-419.

Elkhoury, M., Kiwata, T. & Aoun, E., 2015. Experimental and numerical investigation of a three-dimensional vertical-axis wind turbine with variable-pitch. Journal of Wind Engineering and Industrial Aerodynamics, Volume 139, pp. 111-123.

Fadil, J., Soedibyo & Ashari, M., 2017. Performance analysis of vertical axis wind turbine with variable swept area. s.l., IEEE, 2017 International Seminar on Intelligent Technology and Its Application.

Franchina, N., Kouaissah, O., Persico, G. & Savini, M., 2019. Three-Dimensional CFD Simulation and Experimental Assessment of the Performance of a H-Shape Vertical-AxisWind Turbine at Design and Off-Design Conditions. Int. J. Turbomach. Propuls. Power, 4(30), pp. 1-18.

Hansen, M. O., 2008. Aerodynamics of wind turbines. London: Earthscan.

Jha, A. R., 2011. Wind turbine techonology. New York: CRC Press.

Kostic, C., 2015. Review of the Spalart-Allmaras Turbulence Model and its Modifications to Three-Dimensional Supersonic Configurations. Scientific Technical Review, LXV(1), pp. 43-49 .

Liu, Q. et al., 2019. Effects of trailing-edge movable flap on aerodynamic performance and noise characteristics of VAWT. Energy, Volume 189, p. 116271.

Marinic-Kragic, I., Vicina, D. & Milas, Z., 2019. Concept of flexible vertical-axis wind turbine with numerical simulation and shape optimization. Energy, Volume 167, pp. 841-852.

Nguyen, M. T. et al., 2020. Evaluation of the unsteady aerodynamic forces acting on a vertical-axis turbine by means of numerical simulations and open site experiments. Journal of Wind Engineering & Industrial Aerodynamics, Volume 198, p. 104093.

Peng, H. Y., Han, Z. D., Lin, H. J. & Lam, H. F., 2020. Assessment and optimization of the power performance of twin vertical axis wind turbines via numerical simulations. Renewable Energy, Volume 147, pp. 43-54.

Rezaeiha, A., Kalkman, I. & Blocken, B., 2017. CFD simulation of a vertical axis wind turbine operating at a moderate tip speed ratio: Guidelines for minimum domain size and azimuthal increment. Renewable Energy, Volume 107, pp. 373-385.

Rezaeiha, A., Kalkman, I. & Blocken, B., 2017. Effect of pitch angle on power performance and aerodynamics of a vertical axis wind turbine. Applied Energy, Volume 197, pp. 132-150.

Rezaeiha, A., Montazeri, H. & Blocken, B., 2018. Towards accurate CFD simulations of vertical axis wind turbines at different tip speed ratios and solidities: Guidelines for azimuthal increment, domain size and convergence. Energy Conversion and Management, Volume 156, pp. 301-316.

Satio, D., Utama, I. K. A. P. & Mukhtasor, 2018. The influence of time step setting on the CFD simulation result of vertical axis tidal current turbine. Journal of Mechanical Engineering and Sciences, 122(1), pp. 3399-3409.

Seeni, A. & Rajendran, P., 2019. Numerical Validation of NACA 0009 Airfoil in Ultra-Low Reynolds Number Flows. International Review of Aerospace Engineering (I.RE.AS.E), 12(2), pp. 1973-7459.

Shaheen, M. & Abdallah, S., 2016. Development of efficient vertical axis wind turbine clustered farms. Renewable and Sustainable Energy Reviews, LXIII(1), pp. 237-244.

Shukla, V. & Kaviti, A. K., 2017. Performance evaluation of profile modifications on straight-bladed vertical axis wind turbine by energy and Spalart Allmaras models. Energy, Volume 126, pp. 766-795.

Siddiqui, M. S., Rasheed, A., Kvamsdal, T. & Tabib, M., 2015. Effect of Turbulence Intensity on the Performance of an Offshore Vertical Axis Wind Turbine. Trondheim, Norway, s.n., pp. 312-320.

Zhou, Y., Hou, L. & Huang, D., 2017. The effects of Mach number on the flow separation control of airfoil with a small plate near the leading edge. Computers and Fluids, Volume 156, pp. 274-282.

Zuo, W., Wang, X. & Kang, S., 2016. Numerical simulations on the wake effect of H-type vertical axis wind turbines. Energy, Volume 106, pp. 691-700.

6. Appendices

Appendix A: Complied UDF for the rotating core modelled from its centre of gravity.

```
# include "udf.h"
# include "dynamesh_tools.h"
DEFINE_CG_MOTION(rotate,dt,vel,omega,ti
me,dtime)
{
real freq_t;
omega [2] = freq_t;
}
```

Appendix B:

```
#include "udf.h"

DEFINE_CG_MOTION(yaw, dt, vel, omega,
time, dtime)
{
real a, w, pi;

pi = 3.1415;

/* define motion variables */
a = 0.05; /* 0.05m movement amplitude */
w = 2 * pi * 2; /* 2Hz frequency */

/* define object movement law */
omega [0] = -.5* sin(w*time);
}
```

7. Nomenclature

A	Sweep area [m^2]
c	Blade chord length [m]
C_L	Coefficient of Lift
C_D	Coefficient of Drag
C_P	Coefficient of Power
D	Turbine diameter [m]
dθ	Azimuthal increment [^{0}]
F_L	Lift force [N]
F_D	Drag force [N]
L	Length [m]
H	Blade height [m]
P	Static Pressure [Pa]
Q	Torque [N.m]
R	Radius of rotor [m]
Re	Reynolds number over the blade [-]
U	Wind speed upstream [m/s]
v	Wind velocity [m/s]
V_∞	Wind speed upstream [m/s]

Greek

λ	Tip Speed Ratio (TSR) [-]
ρ	Density of air [kg/m^3]
υ	Kinematic Viscosity [m2/s]
μ	Dynamic Viscosity [$N.s/m^2$]
β	Angle-of-Attack [^{0}]
ω	Angular velocity [rad/sec]

Subscripts

geo	Geometry of the blade
p	Power